Two-photon spectroscopy of neutral barium: Observations of the highly excited even levels and theoretical analysis of the $J = 0$ spectrum

M. Aymar, P. Camus, M. Dieulin, and C. Morillon
Laboratoire Aimé Cotton, Centre National de la Recherche Scientifique II, Bâtiment 505, 91405 Orsay, France
(Received 23 January 1978)

Extensive new data on the even parity $J = 0$ and $J = 2$ levels of neutral barium have been obtained using two-photon absorption spectroscopy with a nitrogen-pumped dye laser and space-charge detection. Members of the Rydberg series $6sns\,^1S_0$ ($16 \leqslant n \leqslant 61$), $6snd\,^1D_2$ ($15 \leqslant n \leqslant 81$), and $6snd\,^3D_2$ ($15 \leqslant n \leqslant 30$) and perturbing levels of these series belonging to the $5d7d$ configuration have been observed; the corresponding wave numbers have been determined. A detailed description of the experimental method is given, followed by the presentation of the new data and the theoretical analysis of the $J = 0$ spectrum. All $J = 0$ levels in the energy range between 34370 cm^{-1} and the first limit were interpreted by means of the multichannel quantum-defect theory. In this energy range, the $6sns\,^1S_0$ series is perturbed by two levels at 38924 and 41441 cm^{-1}; these levels are assigned to $5d6d\,^1S_0$ and $5d7d\,^3P_0$, respectively.

I. INTRODUCTION

In this paper, we describe a two-photon absorption experiment used for studying highly excited even levels of barium and we analyze the data obtained. Preliminary results have already been published by two of us.[1]

The use of a powerful pulsed dye laser allows us to observe two-photon transitions between the ground level and the excited levels with the same parity. The excited levels are observed by detecting the ions created by collisional processes in the vapor, using the space-charge method.[2,3]

Similar experiments have been performed, initially in cesium by Popescu *et al.*[4] and then by other authors in rubidium[5] and in alkaline-earth vapors: calcium[6] and strontium.[7,8]

In Ba, the strong resonant $6s6p\,^1P_0^o$ level at 18060 cm^{-1} and ionization threshold at 42035 cm^{-1} lead to rather high probabilities for two-photon transitions from the ground level $6s^2\,^1S_0$ to the high-lying even $J=0$ and $J=2$ levels. These levels belong either to series $6sns\,^1S_0$ and $6snd\,^{1,3}D_2$ converging on the first $6s(^2S_{1/2})$ limit, or to configurations with two excited valence electrons, low members of the series converging on the $5d\,(^2D_{3/2}, {}^2D_{5/2})$ or the $6p(^2P^o_{1/2}, {}^2P^o_{3/2})$ limits. In Ba, many levels of two valence-electron configurations are localized below the first limit, and thus perturb the Rydberg series. It is therefore of particular interest to analyze these interactions.

Recent measurements of the even $J=0$ and $J=2$ levels of Ba have been made using photographic absorption spectroscopy from excited levels populated with a dye laser.[9,10] Our preliminary observations of this spectrum by two-photon absorption spectroscopy,[1] compared to the preceding ones, showed that better resolution and signal-to-noise ratio are obtained We extend our previous work and determine the energies of the $6sns\,^1S_0$ series ($16 \leqslant n \leqslant 61$), the $6snd\,^1D_2$ series ($15 \leqslant n \leqslant 81$), and the $6snd\,^3D_2$ series ($15 \leqslant n \leqslant 30$). Furthermore, we measure the energies of some perturbing levels which belong to the $5d7d$ configuration.

The even-parity $J=0$ spectrum between 34370 cm^{-1} and 42001 cm^{-1} is analyzed by means of the multichannel quantum defect theory (MQDT).[11-14]

Before presenting experimental results concerning both $J=0$ and $J=2$ spectra (Sec. III) and the MQDT analysis of the $J=0$ spectrum (Sec. IV), we give a detailed discussion of the experimental method (Sec. II).

II. EXPERIMENTAL METHOD

Two-photon absorption spectroscopy takes place in a Ba vapor produced in a heat-pipe cell and illuminated with a pulsed tunable dye laser.

Ions formed essentially by collisional processes[15,16] from the laser-excited atoms in the Ba vapor are detected using the space-charge amplification method in a thermoelectronic diode. The experimental setup is shown in Fig. 1.

A. Dye laser and optical geometry

Initially a S.O.P.R.A (200-kW peak power) and later a Molectron UV-1000 nitrogen pulsed laser were used to pump the dye laser. The dye resonator has been designed in our laboratory.[17] The main elements are, on one side, a concave mirror with a 30% reflectivity and, on the other side, a wavelength-selective device formed by a collimating lens, a prism or a set of prisms used as a beam expander, and a 300-lines/mm grating blazed at 70°.

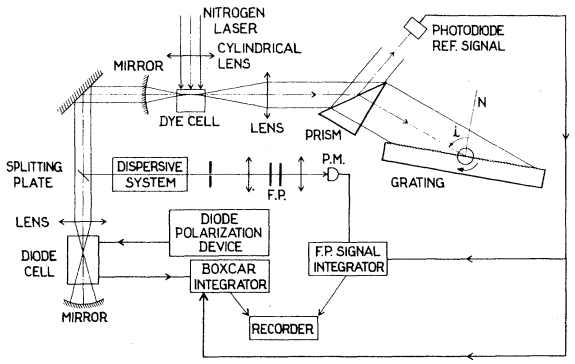

FIG. 1. Experimental setup.

With various coumarines dissolved in ethanol (coumarin 1:7 diethylamino-4-methylcoumarin and coumarin 102:7 amino-4-methylcoumarin), the linewidth [full width at half maximum (FWHM)] achieved is 0.150 cm^{-1} under the best conditions. Typical output power ranges from 1 to 2 kW with a 15-Hz repetition rate. The incident dye-laser beam is focused in the vapor, and reflected by a concave mirror. The laser linewidth is larger than the Doppler width so that the reflected beam is only justified by the best use of the light power. Doppler-free two-photon spectroscopy should be performed with the same experimental setup but using a narrow-band powerful dye system. In order to get a high power density, near 10 kW/cm^2, at the focus, the cell and the focal lengths are as short as possible. In this case, the number of irradiated atoms is small, but the two-photon transition probability increases as the power density squared, so that the total number of transitions is greater.[18]

B. Heat-pipe cell and thermoelectronic diode

The cylindrical heat-pipe cell is the anode of the cylindrical thermoelectronic diode. To prevent corrosion phenomena or chemical reactions, all the parts containing the barium vapor are made of stainless steel. The inner walls of the 190-mm-long pipe (outside diameter: 19 mm) are covered by three layers of 100-fine mesh screen. Both extremities of the tube are connected to the windows by two pairs of o-ring seals which support the water-cooling system, the vacuum- and gas-feeding tubes, and the two holders of the cathodic wire.

The cell is heated over the central part, 80-mm long, by a 300-W electric oven. In the absorption cell, a pure barium vapor or a mixed barium–rare-gas vapor is easily maintained whether the heat-pipe working conditions[19,20] are satisfied or not. In our experiment, argon has always been used as a buffer gas. The usual operating temperature, which ranges from 800 to 900 °C, yields 0.8–2 Torr of barium partial vapor pressure.

The use of a heat-pipe vapor compared to the mixed vapor produced in a classical absorption cell presents two advantages. One is that it minimizes the pressure effects on the Rydberg states by collisions with the buffer-gas atoms. The second is that it stabilizes in time and keeps uniform on its useful length the thermoelectronic emission of the filament by keeping its temperature strictly constant (any fluctuation of the heating power of the oven producing only an increased or decreased length of the vapor column in the heat-pipe working conditions). At the temperature used in the oven, the thermoelectronic emission of the filament polarized to a negative potential is enough to create a space charge, so no other heating process is required.

To a resonant laser light pulse (10^{-8} s) corresponds a fast increase in the current of the diode followed by a slower decrease, as shown in Fig. 2. This decreasing signal is analyzed as the sum of two exponential curves with two different time decays. The first part, with a time constant $\tau_0 \leq 10^{-3}$ s, would be given by the direct capture of negative charges by the anode and positive charges by the filament. The second part, with a longer time constant $\tau_s \simeq 10^{-2}$ s, would give evidence of the imprisonment of positive ions in the space charge.

In order to analyze this positive voltage pulse superposed on a negative continuous potential (the fluctuations of which are essentially due to weak temperature fluctuations of the oven), a well-adapted boxcar integrator has been built in our

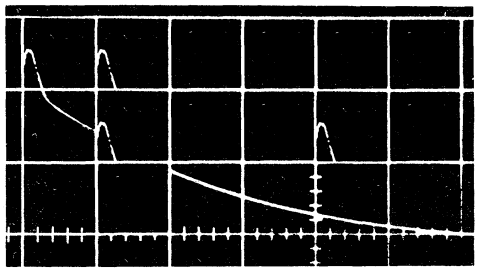

FIG. 2. Diode pulse. Polarization voltage, 300 mV; temperature, 875 °C; Ar pressure, 15 torr; vertical, 10 mV/division, horizontal, 5 msec/division.

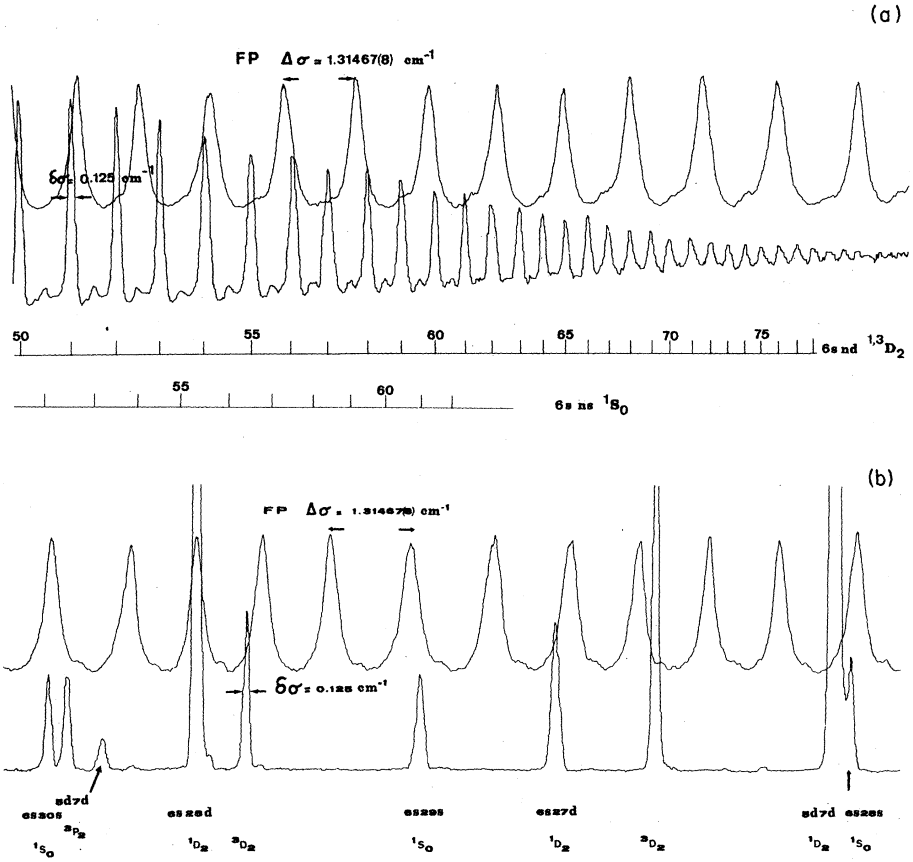

FIG. 3. Two-photon spectrum of Ba I. (a) High members of the $6snd\,^1D_2$ series. (b) In the vicinity of the $5d7d\,^1D_2$ perturber.

laboratory.

Besides the electronic noise, the lack of perfect reproducibility of the laser pulses introduces an uncertainty in the signal value and we integrated n pulses ($n \sim 15$) per point. Typical diode pulses ranging from 0.1 mV to a few hundred mV peak voltage have been detected with this boxcar.

If we consider the amplification factor defined by Marr and Wherrett in their experiment[15] (for one ion, 10^5–10^6 electrons are released from the cathode), this method of detecting two-photon resonances in the vapor is as sensitive as other techniques using photomultipliers to measure the fluorescence light emitted from the excited atoms. In the space-charge detector all the ions created are taken into account, whereas the fluorescence light emitted on the whole space is often received in a small solid angle. Furthermore, only a part of the fluorescence spectrum is usually observed in order to avoid the scattered light from the laser beam.

Finally, the current pulses of the diode are so much longer than the exciting laser pulses and than the emitted light pulses in a fluorescence experiment, that we do not need a fast electronic system.

C. Wave-number calibration

Scanned two-photon absorption resonances were referenced to calibrated transmission maxima of a vacuum-spaced Fabry-Perot interferometer illuminated with a weak part of the dye-laser beam as shown in Fig. 1. The geometrical thickness of the interferometer, defined by silica spacers optically attached to the 60%-reflectivity coated plates has been measured accurately by the method of exact fractions.[21] It gives $1.374\,678 \pm 0.000\,001$ cm^{-1} constant frequency interval between two fringes. Then absolute calibration of the recorded two-photon spectrum is made by reference to the $6s^2\,^1S_0 \rightarrow 6s22d\,^1D_2$ two-photon line, the wave numbers ($41\,740.182 \pm 0.08$ cm^{-1}) of which has been measured using the same method of exact fractions. Finally, the uncertainty on the energies ranges from 0.06 to 0.20 cm^{-1} for several recordings with a maximum possible shift of ± 0.08 cm^{-1} corresponding to the reference wave number determination.

III. RESULTS

The energies of the levels $J=0$ and $J=2$ observed in the range 41 245 cm^{-1} to 42 001 cm^{-1} are given

TABLE I. Observed and calculated even-parity $J=0$ bound states of Ba I. An asterisk indicates a new level.

Designation	E_{obs} (cm^{-1})	Error (cm^{-1})	$E_{obs}-E_{calc}$ (cm^{-1})
$5s8s\,^1S_0$	34 370.984 [a]		−0.353
$6p^2\,^3P_0$	34 493.898 [b]		0.227
$5s9s\,^1S_0$	37 234.185 [a]		0.740
$5d6d\,^3P_0$	37 675.84 [b]		−0.077
$5s10s\,^1S_0$	38 663.746 [a]		−0.081
$5d6d\,^1S_0$	38 923.900 [a]		−0.391
$6s11s\,^1S_0$	39 671.837 [a]		1.614
$6s12s\,^1S_0$	40 233.738 [a]		0.185
$6s13s\,^1S_0$	40 618.194 [a]		−0.342
$6s14s\,^1S_0$	40 891.560 [a]		−0.681
$6s15s\,^1S_0$	41 092.994 [a]		−0.585
$6s16s\,^1S_0$	41 245.163	0.100	−0.651
$6s17s\,^1S_0$	41 362.350	0.100	−0.739
* $5d7d\,^3P_0$	41 441.221	0.090	−0.055
$6s18s\,^1S_0$	41 467.798	0.060	1.605
$6s19s\,^1S_0$	41 535.233	0.060	0.083
$6s20s\,^1S_0$	41 595.895	0.060	0.022
$6s21s\,^1S_0$	41 646.379	0.139	−0.023
$6s22s\,^1S_0$	41 688.729	0.085	−0.014
$6s23s\,^1S_0$	41 724.546	0.060	0.003
$6s24s\,^1S_0$	41 755.001	0.102	−0.075
$6s25s\,^1S_0$	41 781.278	0.060	−0.043
$6s26s\,^1S_0$	41 804.003	0.060	−0.042
$6s27s\,^1S_0$	41 823.818	0.060	−0.031
$6s28s\,^1S_0$	41 841.197	0.100	−0.016
$6s29s\,^1S_0$	41 856.491	0.060	−0.030
$6s30s\,^1S_0$	41 870.092	0.060	0.006
$6s31s\,^1S_0$	41 882.156	0.111	−0.005
* $6s32s\,^1S_0$	41 893.021	0.108	0.062
* $6s33s\,^1S_0$	41 902.733	0.064	0.081
* $6s34s\,^1S_0$	41 911.463	0.119	0.078
* $6s35s\,^1S_0$	41 919.306	0.096	0.023
* $6s36s\,^1S_0$	41 926.434	0.060	−0.013
* $6s37s\,^1S_0$	41 933.055	0.164	0.087
* $6s38s\,^1S_0$	41 938.895	0.060	−0.022
* $6s39s\,^1S_0$	41 944.307	0.060	−0.054
* $6s40s\,^1S_0$	41 949.361	0.078	0.004
* $6s41s\,^1S_0$	41 953.943	0.060	−0.007
* $6s42s\,^1S_0$	41 958.162	0.060	−0.021
* $6s43s\,^1S_0$	41 962.068	0.060	−0.026
* $6s44s\,^1S_0$	41 965.693	0.110	−0.021
* $6s45s\,^1S_0$	41 969.011	0.060	−0.060
* $6s46s\,^1S_0$	41 972.205	0.062	0.015
* $6s47s\,^1S_0$	41 975.098	0.060	0.005
* $6s48s\,^1S_0$	41 977.786	0.060	−0.012
* $6s49s\,^1S_0$	41 980.362	0.100	0.036
* $6s50s\,^1S_0$	41 982.681	0.060	−0.008
* $6s51s\,^1S_0$	41 984.960	0.060	0.057
* $6s52s\,^1S_0$	41 986.968	0.064	−0.011
* $6s53s\,^1S_0$	41 988.982	0.060	0.053
* $6s54s\,^1S_0$	41 990.769	0.077	0.006
* $6s55s\,^1S_0$	41 992.436	0.100	−0.052
* $6s56s\,^1S_0$	41 994.149	0.060	0.032
* $6s57s\,^1S_0$	41 995.683	0.060	0.031
* $6s58s\,^1S_0$	41 997.214	0.150	0.111
* $6s59s\,^1S_0$	41 998.480	0.100	0.005
* $6s60s\,^1S_0$	41 999.735	0.100	−0.038
* $6s61s\,^1S_0$	42 001.026	0.100	0.021

[a] Reference 10.
[b] Reference 26.

TABLE II. Observed even-parity $J=2$ bound states of Ba I. An asterisk indicates a new level.

Designation	Obs. (cm^{-1})	Error (cm^{-1})	Designation	Obs. (cm^{-1})	Error (cm^{-1})
$6s15d\,^3D_2$	41 300.388	0.100	$6s40d\,^1D_2$	41 956.175	0.060
$6s15d\,^1D_2$	41 315.547	0.140	$6s41d\,^1D_2$	41 960.169	0.060
$6s16d\,^3D_2$	41 407.247	0.143	$6s42d\,^1D_2$	41 963.998	0.060
$6s16d\,^1D_2$	41 417.641	0.095	$6s43d\,^1D_2$	41 967.449	0.060
$6s17d\,^3D_2$	41 492.213	0.074	$6s44d\,^1D_2$	41 970.748	0.060
$6s17d\,^1D_2$	41 500.067	0.060	$6s45d\,^1D_2$	41 973.704	0.060
$6s18d\,^3D_2$	41 561.111	0.132	$6s46d\,^1D_2$	41 976.443	0.060
$6s18d\,^1D_2$	41 567.184	0.111	$6s47d\,^1D_2$	41 979.010	0.100
$6s19d\,^3D_2$	41 617.703	0.098	$6s48d\,^1D_2$	41 981.534	0.060
$6s19d\,^1D_2$	41 622.465	0.060	$6s49d\,^1D_2$	41 983.849	0.060
$6s20d\,^3D_2$	41 664.774	0.086	$6s50d\,^1D_2$	41 985.979	0.060
$6s20d\,^1D_2$	41 668.528	0.060	$6s51d\,^1D_2$	41 988.001	0.060
$6s21d\,^3D_2$	41 704.214	0.090	$6s52d\,^1D_2$	41 989.892	0.060
$6s21d\,^1D_2$	41 707.296	0.060	* $6s53d\,^1D_2$	41 991.595	0.060
$6s22d\,^3D_2$	41 737.686	0.060	* $6s54d\,^1D_2$	41 993.304	0.060
$6s22d\,^1D_2$	41 740.182	Étalon wave number	* $6s55d\,^1D_2$	41 994.948	0.060
$6s23d\,^3D_2$	41 766.256	0.060	* $6s56d\,^1D_2$	41 996.415	0.060
$6s23d\,^1D_2$	41 768.349	0.060	* $6s57d\,^1D_2$	41 997.790	0.139
$6s24d\,^3D_2$	41 790.837	0.060	* $6s58d\,^1D_2$	41 999.165	0.094
$6s24d\,^1D_2$	41 792.623	0.089	* $6s59d\,^1D_2$	42 000.382	0.060
$6s25d\,^3D_2$	41 811.935	0.060	* $6s60d\,^1D_2$	42 001.627	0.060
$6s25d\,^1D_2$	41 813.571	0.060	* $6s61d\,^1D_2$	42 002.731	0.060
$6s26d\,^3D_2$	41 829.487	0.083	* $6s62d\,^1D_2$	42 003.830	0.075
$6s26d\,^1D_2$	41 831.906	0.092	* $6s63d\,^1D_2$	42 004.844	0.060
$5d7d\,^1D_2$	41 841.660	0.076	* $6s64d\,^1D_2$	42 005.813	0.060
$6s27d\,^3D_2$	41 848.265	0.060	* $6s65d\,^1D_2$	42 006.720	0.060
$6s27d\,^1D_2$	41 852.055	0.067	* $6s66d\,^1D_2$	42 007.632	0.060
$6s28d\,^3D_2$	41 862.679	0.060	* $6s67d\,^1D_2$	42 008.481	0.116
$6s28d\,^1D_2$	41 864.689	0.067	* $6s68d\,^1D_2$	42 009.292	0.060
$*5d7d\,^3P_2$	41 868.207	0.060	* $6s69d\,^1D_2$	42 010.015	0.100
$*6s29d\,^3D_2$	41 875.490	0.060	* $6s70d\,^1D_2$	42 010.679	0.100
$6s29d\,^1D_2$	41 877.007	0.060	* $6s71d\,^1D_2$	42 011.466	0.100
$*6s30d\,^3D_2$	41 886.856	0.060	* $6s72d\,^1D_2$	42 012.161	0.100
$6s30d\,^1D_2$	41 888.108	0.060	* $6s73d\,^1D_2$	42 012.730	0.100
$6s31d\,^1D_2$	41 898.206	0.067	* $6s74d\,^1D_2$	42 013.315	0.100
$6s32d\,^1D_2$	41 907.371	0.060	* $6s75d\,^1D_2$	42 013.863	0.100
$6s33d\,^1D_2$	41 915.565	0.080	* $6s76d\,^1D_2$	42 014.614	0.100
$6s34d\,^1D_2$	41 923.102	0.060	* $6s77d\,^1D_2$	42 015.131	0.100
$6s35d\,^1D_2$	41 929.828	0.060	* $6s78d\,^1D_2$	42 015.699	0.100
$6s36d\,^1D_2$	41 936.118	0.060	* $6s79d\,^1D_2$	42 016.209	0.100
$6s37d\,^1D_2$	41 941.795	0.060	* $6s80d\,^1D_2$	42 016.671	0.100
$6s38d\,^1D_2$	41 946.985	0.088	* $6s81d\,^1D_2$	42 017.115	0.100
$6s39d\,^1D_2$	41 951.792	0.060			

in Tables I and II; these are the averages of at least two measurements. Members of the $6sns\,^1S_0$ series are observed from $n=16$ to $n=61$ and those of the $6snd\,^1D_2$ series from $n=15$ to $n=81$. These results improve and extend recent observations by Rubbmark *et al.*[10] The observed members of the $6sns\,^1S_0$ and $6snd\,^1D_2$ series have been extended from $n=32$ tp $n=61$ and from $n=53$ to $n=81$, respectively. The level 41 451 cm^{-1} interpreted as $6s18s\,^1S_0$ in Ref. 10 has not been observed. A new $J=0$ level, observed at 41 441 cm^{-1}, is assigned to the $^3P_0$ level of the $5d7d$ configuration. An increased instrumental resolution has allowed us to observe the high members of the series shown in Fig. 3(a) and to separate more clearly than in our previous work[1] the transition corresponding to the $6s28s\,^1S_0$ level at 0.463 cm^{-1} from the strong perturbing $5d7d\,^1D_2$ level [Fig. 3(b)]. A weak two-photon resonance at 41 868 cm^{-1} is identified with the $5d7d\,^3P_2$ level. The intervals between the $^1D_2$ and $^3D_2$ levels of the $6snd$ series are measured up to $n=30$ and are still unresolved for the highest members.

Two signals observed at 41 786.42 cm^{-1} and 41 869.39 cm^{-1} have been identified as two-photon transitions between the ground level $4s^2\,^1S_0$ and

$4p^2\,{}^1S_0$ level of CaI (Ref. 22) and the ground level $5s^2\,{}^1S_0$ and $5s7d\,{}^3D_2$ level of Sr I (Ref. 23), respectively. These two elements are impurities in the 99.9%-pure metallic Ba sample used. Close to the $6s24d\,{}^1D_2$ two-photon signal, a wide line has been observed and is interpreted as a one-photon strontium resonance between the $5s5p\,{}^1P_1^o$ level (populated by the dye fluorescence light) and the $5s9s\,{}^1S_0$ level.

IV. MQDT ANALYSIS OF THE $J=0$ EVEN-PARITY LEVELS

A. Basic formulas of the MQDT analysis

We present here the interpretation of the $J=0$ spectrum by means of the MQDT method introduced by Seaton[11] and reformulated recently by Fano and co-workers.[12-14] Recently, this method has been used to analyze the spectrum of lighter alkaline-earth elements, by Armstrong *et al.*[24] in calcium and by Esherik[8] in strontium. Our study follows these earlier works and consequently we recall here only some basic ideas and formulas of MQDT.

Atoms in excited levels can be considered to consist of an excited electron and of a residual compact ion. The MQDT analysis relies on the existence of a distance r_0 between the electron and the ion such that beyond r_0 the electron moves in a Coulomb potential. For $r \geq r_0$, the wave function of a discrete level is represented as the superposition of the wave function of "collision channels" i, characterized by the state of the ion, the state of the outer electron, and their coupling. The coefficients of the superposition depend upon the short-range interactions (in the non-Coulomb zone $r<r_0$) through parameters μ_α and $u_{i\alpha}$ which characterize the "close-coupling channels" α of the system. The parameters μ_α are the eigenquantum defects associated with the close-coupling channels; the matrix elements $u_{i\alpha}$ provide the unitary transformation between the collision channels i and the close-coupling channels.

These parameters, which are slowly varying functions of energy within the neighborhood of the ionization limits, can be fitted by a semi-empirical analysis of a graphical representation of energy levels.

Following Armstrong *et al.*,[24] we denote by M the number of interacting channels and by N the number of different series limits involved; N is also the number of distinct state of the core in the collision channels.

Each observed level of energy E has N effective quantum numbers ν_i determined from the relations

$$E = I_i - R/\nu_i^2 , \quad i=1,\ldots,N \tag{1}$$

where I_i is the ith ionization limit and R the Rydberg constant of the element.

The $N-1$ independent equations

$$I_i - R/\nu_i^2 = I_j - R/\nu_j^2, \; i \neq j \tag{2}$$

deduced from (1) determine a line $\mathcal{L}$ in the N-dimensional space of the ν_i.

The wave function of an excited level can be expressed in terms of the wave function ψ_α of the close coupling channels:

$$\psi = \sum_\alpha A_\alpha \psi_\alpha \; . \tag{3}$$

The behavior of the wave function at $r \to \infty$ leads to the condition

$$\sum_\alpha A_\alpha u_{i\alpha} \sin\pi(\nu_i + \mu_\alpha) = 0, \quad i=1,\ldots,M \; . \tag{4}$$

The nontrivial solution of (4) requires that:

$$\det\left| u_{i\alpha} \sin\pi(\nu_i + \mu_\alpha) \right| = 0 \; . \tag{5}$$

This equation describes a surface $\mathcal{S}$ in the ν_i space.

Therefore, the theoretical ν_i of the bound levels are obtained as the simultaneous solutions of Eqs. (2) and (5); that is, the positions of bound levels are given by the intersection of the line $\mathcal{L}$ with the surface $\mathcal{S}$. The spectrum analysis thus consists in adjusting the parameters μ_α and $u_{i\alpha}$ so that the theoretical energy values agree with the experimental ones.

The first step of any MQDT treatment is to enumerate the M channels and to decide on the labeling of these channels. The choice of labels should reflect the interactions between channels, which have two principal causes: first, the mixing of different configurations due to Coulomb interaction; second, the mixing, within a given configuration, caused by the spin-orbit coupling. These two effects are important in Ba as in Sr (Ref. 8). The recoupling effects are introduced by considering jj-coupled collision channels. Since the α eigenchannels are nearly LS coupled, an intermediate basis $\bar{\alpha}$ of exactly LS-coupled channels is introduced by writing

$$u_{i\alpha} = \sum_{\bar{\alpha}} u_{i\bar{\alpha}} V_{\bar{\alpha}\alpha} \; , \tag{6}$$

where $u_{i\bar{\alpha}}$ transforms the jj-coupled channel i into the pure LS-coupled channels $\bar{\alpha}$. The $u_{i\bar{\alpha}}$ matrix elements are known analytically. The $V_{\bar{\alpha}\alpha}$ transforms the pure LS-coupled channels $\bar{\alpha}$ into the α

channels for which L and S were useful quantum numbers for designation but not good quantum numbers. The V matrix mainly takes into account the configuration mixing. This $M \times M$ orthogonal matrix can be generated by $\frac{1}{2}[M(M-1)]$ successive rotations in (j,k) planes as described in Appendix B of Ref. 13. Each rotation angle θ_{jk} describes the mixing between two $\bar{\alpha}$ intermediate-basis channels j and k. The θ_{jk} angles will be fitted numerically.

The procedure used in this work to fit theoretical and experimental data is similar to that used in Refs. 24 and 8. We use projections of the quantum-defect plot in the N-dimensional space of the ν_i, on the various planes (ν_i, ν_j). Initial estimates of parameters were obtained by inspection of the projections of the quantum-defect plot. The adjustment of these parameters is performed by minimizing the rms deviation between observed and calculated term values. However the minimization procedure used in our work differs from the one used in the previous works[8,24]; we utilize a nonlinear simplex method.[25]

In addition to energies fitted to experiment, MQDT gives the wave functions of the excited levels.

The coefficients $Z_i^{(n)}$ introduced in the expansion of the wave function $\psi^{(n)}$ of the nth level in terms of the wave functions of the collision channels are given by [24]

$$Z_i^{(n)} = (-1)^{(l_i+1)} \nu_i^{3/2} \sum_\alpha u_{i\alpha} \cos\pi(\nu_i^{(n)} + \mu_\alpha) A_\alpha^{(n)} \frac{1}{N_n}, \tag{7}$$

where N_n is a normalization factor defined in Ref. 13.

B. Results of the MQDT analysis

1. Choice of the MQDT model

The new experimental data obtained for the $J=0$ even-parity spectrum of Ba concern the levels of the $6sns\,^1S_0$ series for n ranging from 16 to 61, and one level perturbing this series. In order to analyze the whole $J=0$ spectrum, we have to consider lower-energy levels. The work of Rubbmark *et al.*[10] provides the energies of the $6sns\,^1S_0$ levels for n ranging from 8 to 15 and of a perturbing level at 38 663 cm^{-1} previously interpreted as $6p^2\,^1S_0$. The energies of $6s^2\,^1S_0$, $6s7s\,^1S_0$, $6p^2\,^3P_0$, $5d^2\,^3P_0$, and $5d6d\,^3P_0$ levels were tabulated by Moore.[26] We have also to consider the $5d^2\,^1S_0$ level, but the energy determination of this level is somewhat ambiguous; indeed the prediction of Palenius[27] at 26 757.4 cm^{-1} is not in agreement with the determination of Vergès[28] at 25 873.83 cm^{-1}.

The channels which are relevant to the analysis of all these $J=0$ levels correspond to Rydberg series converging to the first five limits of the neutral atom: $6s\,^2S_{1/2}$, $5d\,^2D_{3/2,5/2}$, and $6p\,^2P^0_{1/2,3/2}$. This leads to a set of five channels labeled as follows:

1	2	3	4	5
$6s[^2S_{1/2}]ns_{1/2}$	$5d[^2D_{5/2}]nd_{5/2}$	$5d[^2D_{3/2}]nd_{3/2}$	$6p[^2P_{1/2}]np_{1/2}$	$6p[^2P_{3/2}]np_{3/2}$
$6sns\,^1S_0$	$5dnd\,^1S_0$	$5dnd\,^3P_0$	$6pnp\,^3P_0$	$6pnp\,^1S_0$

(8)

In fact, the analysis of the $J=0$ spectrum presented below only concerns the levels higher than 34 370 cm^{-1}; moreover, we consider a MQDT model with only four channels. Before presenting the results of this analysis, we will justify the choice of such restriction.

The low-lying levels below $6s8s\,^1S_0$ ($6s^2\,^1S_0$, $6s7s\,^1S_0$, $5d^2\,^3P_0$, and $5d^2\,^1S_0$) were excluded from the analysis, because a MQDT treatment is unable to accurately fit such levels.[8,24] In fact energies of low-lying levels are affected by core polarization effects. Moreover, for interpreting these levels, far from the ionization limit, energy dependence of parameters cannot be neglected. The analysis of the $J=0$ even bound levels of Ca and Sr has shown that, even a linear dependence of the μ_{ns} quantum defect is insufficient to fit the $ns^2\,^1S_0$ ground level and the first $ns(n+1)s\,^1S_0$ excited level. The interpretation of the low-lying $5d^2$ $J=0$ levels would require the introduction of the energy dependence of quantum defect for channels describing series converging to limits higher than the first limit.

In the energy range from 34 370 cm^{-1} to the first limit, the $6sns\,^1S_0$ series is perturbed by two levels near $6s9s\,^1S_0$ and near $6s17s\,^1S_0$, assigned, respectively, to $6p^2\,^1S_0$ and $5d7d\,^1S_0$ by Rubbmark *et al.*[10] These assignments appear to be questionable. Therefore, in order to obtain a more suitable assignment of these levels, we have done various preliminary fits with different sets of initial parameters corresponding to different labels for the two perturbers. First, we do not introduce mixing between $^1S_0$ and $^3P_0$ levels and try to assign the two perturbers to the channels $5dnd\,^1S_0$ and $6pnp\,^1S_0$. The two perturbers 1 and 2

cannot pertain to the same channel $5dnd\,^1S_0$, since the effective quantum number $\nu^2_{5d_{5/2}} - \nu^1_{5d_{5/2}} \simeq 0.7$ is very different from 0 (mod 1). Since a two-channel MQDT model is unable to interpret the two perturbations, we consider a three-channel MQDT model (channels $i=1,2,5$) where the lower perturber is assinged to $6p^2\,^1S_0$ and the higher one to $5d7d\,^1S_0$ (designations given by Rubbmark[10]). However, with this model, we predict a $5d6d\,^1S_0$ theoretical energy lower than the energy of the $5d6d\,^3P_0$ level tabulated by Moore[26]; therefore, this model would be justified only if the $5d6d\,^3P_0$ energy is inexact. We have also considered a three-channel MQDT model (channels $i=1,2,5$) where the lower perturber is assigned to $5d6d\,^1S_0$ and the higher one to $6p^2\,^1S_0$; we have excluded this hypothesis because it appears more probable that the higher perturber pertains to the $5d7d$ configuration. Moreover Rubbmark *et al.*[10] note that the level at 41 467 cm^{-1} (higher perturber) was observed in absorption from the odd $5d6d\,^3D^o_1$ level; since this latter level does not seem to be mixed with $^1P^o_1$ levels, the level at 41 467 cm^{-1} cannot be a pure $^1S_0$ level. This remark leads us to introduce the $5dnd\,^3P_0$ channels in the MQDT model. The best interpretation of all $J=0$ levels above 34 370 cm^{-1}, $6p^2\,^3P_0$ excepted, is obtained with a three-channel MQDT model (channels $i=1,2,3$), the perturbers being assigned to $5d6d\,^1S_0$ and $5d7d\,^3P_0$. In order to interpret the $6p^2\,^3P_0$ level we introduce an additional channel: since the $6sns\,^1S_0$ levels are not perturbed by a $6pnp\,^1S_0$ level, we consider only one $6p[^2P]np$ channel instead of the two channels 4 and 5 and use the average value of the two $^2P^o_{1/2,3/2}$ limits.

2. *Final results of the MQDT analysis*

Now we present the results of our latest MQDT analysis of all $J=0$ levels above 34 370 cm^{-1}, that is, the $6sns\,^1S_0$ levels for n ranging from 8 up to 61, the two perturbers $5d6d\,^1S_0$ and $5d7d\,^3P_0$, and, in addition, the $6p^2\,^3P_0$ and $5d6d\,^3P_0$ levels. It is expected that the two last levels do not perturb the $6sns\,^1S_0$ series very much. The energies of studied levels are compiled in Table I.

a. Optimal set of parameters. The optical set of MQDT parameters is given in Table III. These parameters are obtained by excluding from the fit the high-lying levels $6sns\,^1S_0$ for $n \geq 45$ and by using a revised value for the first ionization limit $I_{6s} = 42\,035.04$ cm^{-1}; this will be discussed below

TABLE III. MQDT parameters for even-parity $J=0$ bound states.

$i, \bar{\alpha}, \alpha$	1	2	3	4
$\lvert i\rangle$	$6s[^2S_{1/2}]ns_{1/2}$	$5d[^2D_{5/2}]nd_{5/2}$	$5d[^2D_{3/2}]nd_{3/2}$	$6p[^2P]np$
I_i	42 035.04	47 709.86	46 908.89	63 423.84
$\lvert\bar{\alpha}\rangle$	$6sns\,^1S_0$	$5dnd\,^1S_0$	$5dnd\,^3P_0$	$6pnp\,^3P_0$
μ_α	0.1817	0.4224	0.6185	0.0524
$\frac{d\mu_\alpha}{d\epsilon}$	0.3981	0	0	0
$u_{i\bar{\alpha}}$	1	0	0	0
	0	$(3/5)^{1/2}$	$-(2/5)^{1/2}$	0
	0	$+(2/5)^{1/2}$	$(3/5)^{1/2}$	0
	0	0	0	1
$V_{\alpha\bar{\alpha}}$	0.9628	−0.2677	0.0372	0.0003
	0.2693	0.9390	−0.2137	0
	0.0223	0.2157	0.9761	−0.0138
	0	0.0030	0.0135	0.9999
	$\theta_{12} = 0.2728$	$\theta_{23} = 0.2175$	$\theta_{13} = 0.0223$	$\theta_{34} = 0.0138$
$u_{i\alpha}$	0.9628	−0.2677	0.0372	0.0003
	0.1945	0.5910	−0.7828	0.0088
	0.1876	0.7610	0.6210	−0.0107
	0	0.0030	0.0135	0.9999

TABLE IV. Admixture coefficients per state of the $\bar{\alpha}$ intermediate-basis set, $Z^2_{\bar{\alpha}}$.

Energy	$[Z_{6sns\,^1S_0}]^2$	$[Z_{5dnd\,^1S_0}]^2$	$[Z_{5dnd\,^3P_0}]^2$	Designation
34 370.984	0.975	0.017	0.000	$6s8s\,^1S_0$
37 234.185	0.977	0.016	0.003	$6s9s\,^1S_0$
37 675.84	0.005	0.009	0.985	$5d6d\,^3P_0$
38 663.746	0.624	0.369	0.006	$6s10s\,^1S_0$
38 923.900	0.417	0.577	0.003	$5d6d\,^1S_0$
39 671.837	0.982	0.016	0.000	$6s11s\,^1S_0$
41 362.350	0.975	0.006	0.018	$6s17s\,^1S_0$
41 441.221	0.347	0.069	0.583	$5d7d\,^3P_0$
41 467.798	0.715	0.018	0.266	$6s18s\,^1S_0$
41 535.233	0.984	0.000	0.016	$6s19s\,^1S_0$

(Sec. IV B 2 *d*). A linear energy dependence is involved for the μ_{6s} quantum eigendefect; we have

$$\mu_{6s} = \mu_1 + \frac{d\mu_1}{d\epsilon}\,\epsilon\ ,$$

with $\epsilon = 1/\nu^2_{6s}$.

The 4×4 unitary matrix V depends upon six angles θ_{jk}. We found that the studied levels could be fitted accurately by setting $\theta_{14}=\theta_{24}=0$ and by adjusting the four remaining angles. We factor the V matrix in the form

$$V = \mathcal{R}_{12}(\theta_{12})\mathcal{R}_{13}(\theta_{13})\mathcal{R}_{34}(\theta_{34})\mathcal{R}_{23}(\theta_{23})\ .$$

The V matrix was initially assumed to mix only the $\bar{\alpha}$ channels with identical values of L and S, that is $\theta_{13}=\theta_{23}=\theta_{14}=\theta_{24}=0$. However the introduction of couplings between the $5dnd\,^1S_0$ and $5dnd\,^3P_0$ channels ($\theta_{23}\neq 0$) and also between the $6sns\,^1S_0$ and $5dnd\,^3P_0$ channels ($\theta_{13}\neq 0$) significantly improve the fit. This means that the mixing of the $\bar{\alpha}$ channels is due not only to electrostatic interaction but also to spin-orbit coupling.

b. Wave functions. The admixture Z^2_i of channel i present in each of the bound states has been calculated with the parameters of Table III using Eq. (7). Since the bound states of Ba are best described in terms of LS coupling, we transform the Z_i coefficients into the $\bar{\alpha}$ basis, that is,

$$Z_{\bar{\alpha}} = \sum_i Z_i\, u_{i\bar{\alpha}}\ .$$

The mixing of the $6pnp\,^3P_0$ channel with the three other channels is very small: for the $6p^2$ level $(Z_{6pnp\,^3P_0})^2 = 0.999$, and for the other levels $(Z_{6pnp\,^3P_0})^2$ is always smaller than 1.10^{-3}. The $6p^2\,^3P_0$ is a pure level. We have verified that a three-channel MQDT model, neglecting the last $6pnp\,^3P_0$ channel, gives nearly the same results as those presented here.

In Table IV we have tabulated the admixture coefficients of the first three channels present in some levels. For all levels not reported in Table IV we have $(Z_{6sns\,^1S_0})^2 > 0.99$. We note that the $5d6d\,^3P_0$ is, as expected, nearly a pure level. It also appears that the admixture of the perturbing levels into the $6sns\,^1S_0$ series is very strongly localized. The two levels at 38 663 and 38 923 cm^{-1} are strongly mixed; the best suitable designations of these levels correspond respectively to $6s10s\,^1S_0$ and to $5d6d\,^1S_0$. Levels at 41 441 and 41 467 cm^{-1} are, respectively, assigned to the $5d7d\,^3P_0$ and $6s18s\,^1S_0$ levels.

c. Interpretation of energy levels. The MQDT model allows us to interpret the 58 levels in the energy range studied with a rms deviation $\overline{\Delta E} = 0.41\ cm^{-1}$. The theoretical term values calculated with this model are compared with experimental data in Table I.

Figure 4(a) shows a projection of the three-dimensional quantum-defect plot on the $(\nu_{6s}, \nu_{5d_{3/2}})$ plane; one has $-\nu_{6s}$ (mod 1) vs $\nu_{5d_{3/2}}$. The solid line is calculated with the optimal set of parameters of Table III. Note on the Figure that the vertical branch at $\nu_{5d_{3/2}} = 2.973$ corresponds to the $6p^2\,^3P_0$ level, and we see that this level does not perturb the $6sns\,^1S_0$ series.

For various reasons discussed above (Sec. IV B1), the low-lying levels were excluded from the MQDT fit. By extending the curve plotted in Fig. 4(a) in the region where $\nu_{5d_{3/2}}$ lies between 1.5 and 2.8, it could be seen that the low-lying levels are badly interpreted as expected; in particular, the perturbation by the $5d^2\,^1S_0$ level, awaited for below the $6s7s\,^1S_0$ level, is shifted towards higher energy. However, by invoking a large energy dependence of the quantum defects μ_2 and μ_3, we are able to approximately fit the four low-lying levels, though the fit to the high-lying levels is somewhat impaired. But bound-state data are insufficient to obtain a precise determination of such an energy dependence, as shown in Ref. 24; moreover, the determination of the $5d^2\,^1S_0$ level is ambiguous. The fit of all $J=0$ levels could be perhaps improved with new

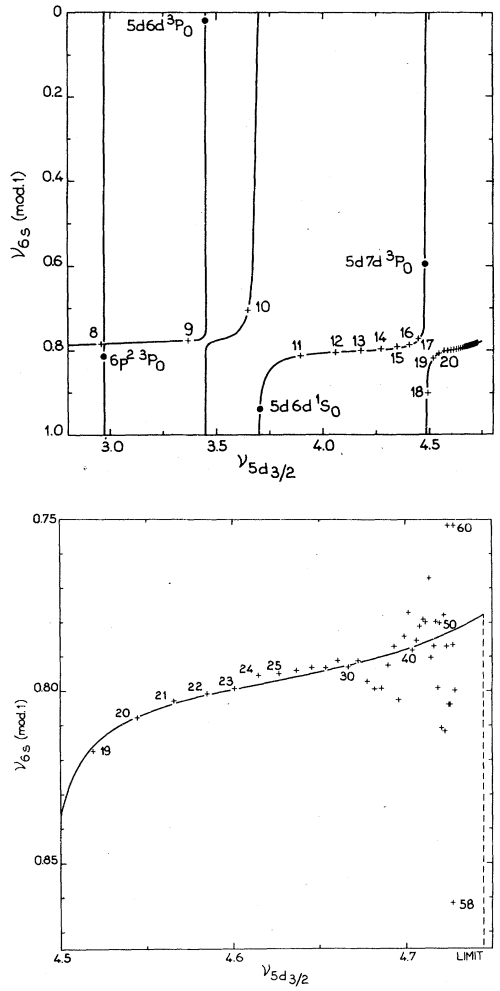

FIG. 4. Lu-Fano plot of the $J=0$ even bound states of Ba I. (a) Quantum-defect plot for the $J=0$ levels above $6s8s\ ^1S_0$. (b) Expanded quantum-defect plot of the $J=0$ data near the first ionization limit.

data on the relevant autoionizing spectra.

d. Ionization limit. For the high-lying levels, the determination of the ν_{6s} effective quantum number strongly depends on the value of the ionization limit I_{6s}. Garton and Tomkins[29] have previously given $I_{6s}=42\,035.14\pm0.05$ cm^{-1}. Rubbmark *et al.*[10] have found it necessary to decrease this value by 0.29 cm^{-1}. Taking into account the uncertainty in the I_{6s} value, we have excluded the high-lying levels $6sns\ ^1S_0$ for $n\geq45$ from the fit which gives the optimal set of MQDT parameters, but we have carried out various fits with different values of the I_{6s} limit. The best interpretation of the high-lying levels is obtained with the value $I_{6s}=42\,035.04$. Moreover, this revised value is confirmed by a one-channel quantum-defect analysis of the high-lying levels of the $6snd\ ^1D_2$ series for n ranging from 29 up to 81. This analysis is done by using the procedure developed by Seaton in Ref. 30; a least-squares fitting of experimental energies to theoretical values depending on three parameters provides $I_{6s}=42\,035.04\pm0.05$ cm^{-1} in perfect agreement with the value obtained by the analysis of the $J=0$ levels. The error on the fitted I_{6s} value is smaller than the experimental uncertainty on the reference wave number determination which is 0.08 cm^{-1}.

Figure 4(b) shows the quantum-defect plot of the high-lying $J=0$ levels with $\nu_{5d_{3/2}}\geq4.5$. The high-lying levels excluded from the fit ($n\geq45$) appear to deviate from the theoretical curve; however, the differences between measured and calculated energies are always smaller than the experimental uncertainty, as can be seen in Table I. Apparently the $6s58s$ level deviates much more than the other levels from the theoretical curve, but it must be noticed that the experimental error is particularly large for this level. The very good agreement obtained for all levels but $6s58s$ can only be obtained by using the revised value $I_{6s}=42\,035.04$ cm^{-1}. A possible shift of ±0.08 cm^{-1} could be expected for this value owing to the uncertainty of the reference wave number determination, but this shift has no consequence on the Lu-Fano plot, since the ν_{6s} quantum numbers are not modified.

V. CONCLUSION

In addition to the previous work on Ba, two-photon absorption spectroscopy and space-charge detection of ions have allowed us to extend the knowledge of the levels of the even $J=0$ and $J=2$ spectra. For the $J=0$ levels, the energy values are accurately fitted by a four-channel MQDT model. The $J=2$ spectrum presents a more complicated scheme of interacting levels which could be studied only by considering a MQDT model with a great number of channels. The $6snd\ ^1D_2$ and $6snd\ ^3D_2$ Rydberg series exhibit a mutual interaction; moreover, these series are perturbed by various levels, mainly belonging to configurations $5dns$ and $5dnd$. Owing to the departure from LS coupling, six channels are relevant to the study of the $J=2$ members of series converging on the $5d\ ^2D_{3/2,5/2}$ limits. The MQDT analysis of the $J=2$ spectrum is in progress and will be reported later. For a detailed MQDT analysis, an increased resolution power is needed to measure the separation between the $^1D_2$ and $^3D_2$ levels of the $6snd$ upper members. Consequently, a Doppler-free two-photon absorption experiment with a narrow-linewidth dye laser is being performed in our laboratory.

ACKNOWLEDGMENTS

We are grateful to Dr. S. Feneuille for his stimulating interest. We thank Mrs. R. Baronnet and M. Oppenheimer for giving us technical assistance in the several phases of the experimental work and A. Raynal, who participated in the preliminary experimental investigations.

Thanks are also due to A. Richard who has made the electronic boxcar integrator which has played a great role in the presented results.

[1]P. Camus and C. Morillon, J. Phys. B 10, L133 (1977).
[2]P. D. Foote and F. L. Mohler, Phys. Rev. 26, 195 (1925).
[3]E. Badareu, I. Popescu, C. Ghiță, and G. Musa, Rev. Roum. Phys. 10, 785 (1965).
[4]D. Popescu, C. B. Collins, B. W. Johnson, and I. Popescu, Phys. Rev. 19, 1182 (1974); S. M. Curry, C. B. Collins, M. Y. Mirza, D. Popescu, and I. Popescu, Optics Commun. 16, 251 (1976).
[5]Y. K. Kato and B. P. Stoïcheff, J. Opt. Soc. Am. 66, L490 (1976).
[6]P. Esherick, J. A. Armstrong, R. W. Dreyfus, and J. J. Wynne, Phys. Rev. Lett. 36, 1296 (1976).
[7]P. Ewart and A. F. Purdie, J. Phys. B 9, L437 (1976).
[8]P. Esherick, Phys. Rev. A 15, 1920 (1977).
[9]D. J. Bradley, P. Ewart, J. V. Nicholas, and J. R. D. Shaw, J. Phys. B 6, 1594 (1973).
[10]J. R. Rubbmark, S. A. Borgström, and K. Bockasten, J. Phys. B 10, 421 (1977).
[11]M. J. Seaton, Proc. Phys. Soc. (Lond.) 88, 801 (1966).
[12]K. T. Lu and U. Fano, Phys. Rev. A 2, 81 (1970).
[13]C. M. Lee and K. T. Lu, Phys. Rev. A 8, 1241 (1973).
[14]U. Fano, J. Opt. Soc. Am. 65, 979 (1975).
[15]G. V. Marr and S. R. Wherrett, J. Phys. B 5, 1735 (1972).
[16]D. Popescu, M. L. Pascu, C. V. Collins, B. W. Johnson, and I. Popescu, Phys. Rev. A 8, 1666 (1973).
[17]D. H. Tuan, S. Liberman, and J. Pinard, Opt. Commun. 18, 533 (1976).
[18]B. Gagnac, G. Grynberg, and F. Biraben, J. Phys. 34, 845 (1973).
[19]Y. Eastman, Sci. Am. 218, 38 (1968).
[20]C. R. Vidal and J. Cooper, J. Appl. Phys. 40, 3370 (1969).
[21]R. S. Longhurst, *Geometrical and Physical Optics* (Longmans, Green, New York, 1957).
[22]C. E. Moore, *Atomic Energy Levels*, Natl. Bur. Stand. (U.S.) Circ. No. 467 (U.S. GPO, Washington D. C., 1949), Vol. I.
[23]C. E. Moore, *Atomic Energy Levels*, Natl. Bur. Stand. (U.S.) Circ. No. 467 (U.S. GPO, Washington D. C., 1952), Vol. II.
[24]J. A. Armstrong, P. Esherick, and J. J. Wynne, Phys. Rev. A 15, 180 (1977).
[25]J. A. Nelder and R. Mead, Comput. J. 7, 308 (1965).
[26]C. E. Moore, *Atomic Energy Levels*, Natl. Bur. Stand. (U.S.) Circ. No. 467 (U.S. GPO, Washington, D. C., 1958), Vol. III.
[27]H. P. Palenius, Phys. Lett. A 56, 451 (1976).
[28]J. Vergès (private communication).
[29]W. R. S. Garton and F. S. Tomkins, Astrophys. J. 158, 1219 (1969).
[30]M. J. Seaton, Proc. Phys. Soc. (Lond.) 88, 815 (1966).

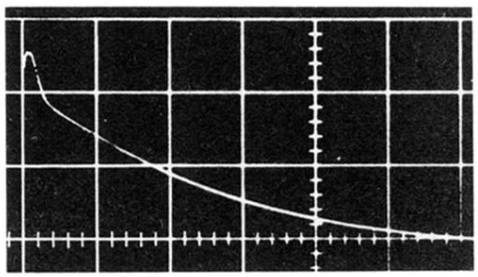

FIG. 2. Diode pulse. Polarization voltage, 300 mV; temperature, 875 °C; Ar pressure, 15 torr; vertical, 10 mV/division, horizontal, 5 msec/division.